Influence of Microscale Turbulent Droplet Clustering on Radar Cloud Observations

KEIGO MATSUDA AND RYO ONISHI

Center for Earth Information Science and Technology, Japan Agency for Marine-Earth Science and Technology, Yokohama, Japan

MASAAKI HIRAHARA AND RYOICHI KUROSE

Department of Mechanical Engineering and Science, Kyoto University, Kyoto, Japan

KEIKO TAKAHASHI

Center for Earth Information Science and Technology, Japan Agency for Marine-Earth Science and Technology, Yokohama, Japan

SATORU KOMORI

Department of Mechanical Engineering and Science, Kyoto University, Kyoto, Japan

(Manuscript received 20 November 2013, in final form 5 May 2014)

ABSTRACT

This study investigates the influence of microscale turbulent clustering of cloud droplets on the radar reflectivity factor and proposes a new parameterization to account for it. A three-dimensional direct numerical simulation of particle-laden isotropic turbulence is performed to obtain turbulent clustering data. The clustering data are then used to calculate the power spectra of droplet number density fluctuations, which show a dependence on the Taylor microscale-based Reynolds number (Re_λ) and the Stokes number (St). First, the Reynolds number dependency of the turbulent clustering influence is investigated for $127 < \mathrm{Re}_\lambda < 531$. The spectra for this wide range of Re_λ values reveal that $\mathrm{Re}_\lambda = 204$ is sufficiently large to be representative of the whole wavenumber range relevant for radar observations of atmospheric clouds. The authors then investigate the Stokes number dependency for $\mathrm{Re}_\lambda = 204$ and propose an empirical model for the turbulent clustering influence assuming power laws for the number density spectrum. For Stokes numbers less than 2, the proposed model can estimate the influence of turbulence on the spectrum with an RMS error less than 1 dB when calculated over the wavenumber range relevant for radar observations. For larger Stokes number droplets, the model estimate has larger errors, but the influence of turbulence is likely negligible in typical clouds. Applications of the proposed model to two idealized cloud observing scenarios reveal that microscale turbulent clustering can cause a significant error in estimating cloud droplet amounts from radar observations with microwave frequencies less than 13.8 GHz.

1. Introduction

Clouds play crucial roles in the heat and water systems of Earth. To improve our understanding of cloud physics, a large number of observational studies have been conducted to estimate the spatial distribution of cloud microphysical properties, such as the cloud water mixing ratio and the effective droplet radius. Radar is one of the most powerful tools since it can provide two- or three-dimensional estimates of cloud microphysical properties over a large domain (Okamoto et al. 2007; Stephens et al. 2008; Ellis and Vivekanandan 2011). In radar observations, microwave radiation is transmitted from an antenna toward a target cloud and the reflected microwaves received and analyzed. The relation between the transmitted power P_t and the received power P_r of the microwaves is given by the following radar equation:

$$P_r = \frac{P_t G^2 k_m^2 |K|^2 V}{4^5 R^4} Z, \tag{1}$$

Corresponding author address: Keigo Matsuda, Center for Earth Information Science and Technology, Japan Agency for Marine-Earth Science and Technology, 3173-25 Showa-machi, Kanazawa-ku, Yokohama, Kanagawa 236-0001, Japan.
E-mail: k.matsuda@jamstec.go.jp

DOI: 10.1175/JAS-D-13-0368.1

where G is the antenna gain, k_m is the microwave wavenumber, R is the distance between the antenna and the cloud, K is the dielectric coefficient of a water droplet, V is the measurement volume, and Z is the radar reflectivity factor ($\mathrm{mm^6\,m^{-3}}$). Crucially, Z is dependent on the cloud microphysical properties, implying that cloud properties can be estimated from Z.

The relation between Z and cloud microphysical properties is explained by two mechanisms: incoherent scattering and coherent scattering. Incoherent scattering occurs when the cloud droplets are dispersed randomly and uniformly (Bohren and Huffman 1983). The radar reflectivity factor for the incoherent scattering case is proportional to the sum of the Rayleigh scattering intensity from each droplet and independent of the microwave frequency f_m. On the other hand, coherent scattering—often referred to as Bragg scattering—occurs when the droplets are distributed nonuniformly. The nonuniform distribution causes the interference of scattered microwaves, which in turn increases the radar reflectivity factor obtained from Eq. (1). This coherent scattering by discrete particles is more specifically referred to as "particulate" Bragg scattering (Kostinski and Jameson 2000). Coherent scattering can also be caused by a nonuniform distribution of the refractive index of clear air—which may be referred to as "clear-air Bragg scattering." Most studies assume that particulate Bragg scattering is insignificant in atmospheric clouds (Gossard and Strauch 1983). However, this assumption is contradicted by the observations of developing cumulus clouds by Knight and Miller (1993) and Knight and Miller (1998). They observed significant differences between the radar reflectivity factors for 10- and 3-cm microwaves, which are classified in the S and X bands, respectively. A similar wavelength dependency of the radar reflectivity factor was found for the case of smoke plumes from an intense industrial fire by Rogers and Brown (1997), who compared the data observed by a UHF wind profiler (wavelength 32.8 cm) and an X-band radar (3.2 cm). Knight and Miller (1998) explained that these differences resulted from coherent scattering by nonuniform cloud droplet concentrations created by the turbulent mixing of cloud with environmental clear air (i.e., turbulent entrainment). That is, they attributed the differences to the large-scale nonuniform distribution of cloud droplets. Erkelens et al. (2001) investigated the influence of turbulent entrainment on the observations of Knight and Miller (1998). They analyzed the observational data using an equation for clear-air Bragg scattering based on the $-5/3$ power law of scalar concentration spectra in turbulence and concluded that turbulent entrainment is not the only relevant factor for coherent scattering in cumulus clouds. Kostinski and Jameson (2000) pointed out that microscale turbulent droplet clustering is also a cause of coherent scattering in cumulus clouds. The turbulent clustering is caused by an inertial effect of particles within turbulent flows, which generates microscale nonuniform particle distributions, often referred to as preferential concentration (Maxey 1987; Squires and Eaton 1991; Wang and Maxey 1993; Chen et al. 2006). Note that turbulent clustering can occur even without large-scale nonuniform particle distributions. Many authors have investigated the effect of turbulent clustering on collisions of cloud droplets (e.g., Sundaram and Collins 1997; Pinsky and Khain 1997; Reade and Collins 2000; Ayala et al. 2008b,a; Onishi et al. 2009; Woittiez et al. 2009; Wang et al. 2009; Jin et al. 2010; Onishi and Vassilicos 2014). The possible importance of turbulent clustering for the radar reflectivity factor, however, was first suggested by Kostinski and Jameson (2000). Recently, Dombrovsky and Zaichik (2010) estimated the influence of turbulent clustering based on the semi-analytical clustering model of Zaichik and Alipchenkov (2007). Their estimate indicated that turbulent clustering considerably increases the radar reflectivity factor. These studies clearly suggest that the influence of turbulence should be carefully considered to obtain reliable estimates of cloud microphysical properties from radar observations. However, until now there has been no reliable way to estimate this influence. One recent approach is that of Dombrovsky and Zaichik (2010), but their estimate relied on a highly simplified clustering model that adopted a simple extrapolation for large scales.

This study, therefore, aims to investigate the influence of microscale turbulent clustering on the radar reflectivity factor and construct a reliable model for estimating it. A three-dimensional direct numerical simulation (DNS) of particle-laden isotropic turbulence is performed in order to obtain turbulent clustering data, and then the influence of turbulence is analyzed and modeled. The model is then applied to two idealized radar observation scenarios to assess the influence quantitatively.

2. Computational method

a. Air turbulence

The governing equations of turbulent airflow are the continuity and Navier–Stokes equations for three-dimensional incompressible flows:

$$\frac{\partial u_i}{\partial x_i} = 0, \tag{2}$$

$$\frac{\partial u_i}{\partial t} + \frac{\partial u_i u_j}{\partial x_j} = -\frac{1}{\rho_a}\frac{\partial p}{\partial x_i} + \nu\frac{\partial^2 u_i}{\partial x_j \partial x_j} + F_i, \tag{3}$$

where u_i is the fluid velocity in the ith direction, ρ_a is the air density, p is the pressure, ν is the kinematic viscosity, and F_i is the external forcing term.

The fourth-order central-difference scheme (Morinishi et al. 1998) was used for the advection term and the second-order Runge–Kutta scheme was used for time integration. The velocity and pressure were coupled by the highly simplified marker and cell (HSMAC) method (Hirt and Cook 1972). Statistically steady-state turbulence was formed by applying an external forcing using the reduced-communication forcing (RCF) method of Onishi et al. (2011), which maintains the intensity of large-scale eddies while keeping a high parallel efficiency.

It should be noted that atmospheric turbulence is typically neither homogeneous nor isotropic. However, the assumptions of homogeneity and isotropy are reasonable for the small scales corresponding to the wavenumber range relevant to radar observations (see section 4a). Although energy-containing large-scale eddies generate large-scale inhomogeneity and anisotropy, dissipative small-scale eddies work to flatten the inhomogeneities, leading to local homogeneity and isotropy. This local homogeneity assumption is the basis of most turbulence models.

b. Droplet motions

Droplet motions are tracked by the Lagrangian method. The governing equation for droplet motion is

$$\frac{dv_i}{dt} = -\frac{v_i - u_i}{\tau_p} + g_i, \tag{4}$$

where v_i is the particle velocity in the ith direction, τ_p is the droplet relaxation time, and g_i is the gravitational acceleration in the ith direction (Onishi et al. 2009; Woittiez et al. 2009; Wang et al. 2009; Jin et al. 2010; Onishi et al. 2013). Equation (4) is based on the following two assumptions: (i) the droplets are Stokes particles [i.e., spherical with small particle Reynolds numbers ($\mathrm{Re}_p \equiv 2r_p|\mathbf{u} - \mathbf{v}|/\nu$)] and (ii) the ratio of the density of droplets to that of the surrounding air is much larger than unity (Maxey and Riley 1983; Kim et al. 1998). The relaxation time for the Stokes particle is given by

$$\tau_p = \frac{\rho_p}{\rho_a}\frac{2r_p^2}{9\nu}. \tag{5}$$

In clouds, turbulent modulation and the frequency of droplet collisions likely remain small since the volume fraction ϕ is smaller than 10^{-6}. Thus, these effects were neglected for simplicity (Matsuda et al. 2012).

TABLE 1. Numerical conditions and flow properties: u_{rms} is the RMS value of velocity fluctuation, Re is the Reynolds number defined as $\mathrm{Re} = L_0U_0/\nu$, Re_λ is the turbulent Reynolds number defined as $\mathrm{Re}_\lambda = l_\lambda u_{\mathrm{rms}}/\nu$, l_λ is the Taylor microscale, $k_{\max}$ is the maximum wavenumber given by $k_{\max} = N_g/(2L_0)$, and l_η is the Kolmogorov scale.

N_g	L_0 (m)	u_{rms} (m s^{-1})	Re	Re_λ	$k_{\max}l_\eta$
256	0.0200	0.274	360	127	2.01
512	0.0400	0.345	909	204	2.02
1000	0.0666	0.499	2220	322	2.06
2000	0.1560	0.544	5595	531	2.07

c. Computational conditions

The computational domain was set to a cube with edges of length $2\pi L_0$, where L_0 is the representative length scale. Periodic boundary conditions were applied in all three directions. The domain was discretized uniformly into N_g^3 grid points, giving a grid spacing of $\Delta = 2\pi L_0/N_g$. The DNS was performed for four turbulent flows, each with a different value of the Taylor-microscale-based turbulent Reynolds number, defined as $\mathrm{Re}_\lambda = l_\lambda u_{\mathrm{rms}}/\nu$, where u_{rms} is the RMS value of the velocity fluctuations and l_λ is the Taylor microscale. Table 1 shows the computational parameters for the air turbulence simulations and the statistical results obtained. The kinematic viscosity was set to 1.5×10^{-5} m^2 s^{-1}. Note that the flow conditions are the same as those of Onishi et al. (2011), who showed that turbulent flows are well resolved under all the chosen conditions. Since the resolutions were chosen to satisfy $k_{\max}l_\eta \approx 2$, where $k_{\max}$ is the maximum wavenumber given by $k_{\max} = N_g(2L_0)^{-1}$, in our DNS experiments the nondimensional energy dissipation rate was essentially the same for all the flows.

The droplet radius r_p was varied so that the Stokes number, defined as $\mathrm{St} = \tau_p/\tau_\eta$, where $\tau_\eta = (\nu/\epsilon)^{1/2}$ is the Kolmogorov time scale, took values of 0.05, 0.1, 0.2, 0.5, 1.0, 2.0, and 5.0. The droplet radii for St = 1.0 were 22.9, 23.1, 20.2, and 23.4 μm for Re_λ = 127, 204, 322, and 531, respectively. The number of droplets was set to 8×10^6, 1.5×10^7, 5×10^7, and 5×10^7 for Re_λ = 127, 204, 322, and 531, respectively. For most of the simulations, the gravitational accelerations g_i were set to zero in order to focus on the Re_λ and St dependencies of turbulent clustering. However, we have also performed DNS experiments with $(g_1, g_2, g_3) = (0, g, 0)$, where $g = 9.8$ m s^{-2}, to investigate the influence of gravitational droplet settling. Details of the numerical conditions are described in section 4d.

The code is fully parallelized for a three-dimensional domain decomposition using a Message Passing Interface (MPI) library (Onishi et al. 2013). The largest simulation

(i.e., the case $\mathrm{Re}_\lambda = 531$) was performed on 32 nodes of the Earth Simulator 2 supercomputer operated by the Japan Agency for Marine-Earth Science and Technology (JAMSTEC).

3. Radar reflectivity factor

The intensity of reflected microwaves is determined by the scattering intensity of each droplet and the interference between scattered microwaves. Since the radii of cloud droplets are much smaller than the wavelength of the microwaves, the scattering is classified as Rayleigh scattering, which gives intensities proportional to r_p^6. In the case where droplets are randomly and uniformly dispersed—implying zero spatial correlations between droplets—the effects of interference cancel and become zero. Thus, the radar reflectivity factor for randomly and uniformly located monodispersed droplets Z_{random} is given by

$$Z_{\mathrm{random}} = 2^6 r_p^6 n_p, \tag{6}$$

where n_p is the droplet number density. Note that Z_{random} is independent of k_m. In the alternative case, where droplets form clusters, the effect of interference appears as an additional term and the radar reflectivity factor becomes dependent on k_m. The radar reflectivity factor for monodispersed clustering droplets Z_{cluster} is given by

$$Z_{\mathrm{cluster}} = Z_{\mathrm{random}} + \frac{2^7 \pi^2 r_p^6}{\kappa^2} E_{\mathrm{np}}(\kappa), \tag{7}$$

where κ is the absolute value of the difference between the incident and scattered wavenumber vectors $\mathbf{k}_{\mathrm{inc}}$ and $\mathbf{k}_{\mathrm{sca}}$; that is, $\kappa = |\mathbf{k}_{\mathrm{inc}} - \mathbf{k}_{\mathrm{sca}}|$ (Gossard and Strauch 1983; Erkelens et al. 2001). Because the antenna receives backward scattering, κ becomes $2k_m$, providing the Doppler effect is small enough. The power spectrum of droplet number density fluctuations $E_{\mathrm{np}}(k)$ represents the intensity of clustering for wavenumber k. It should be noted that Eq. (7) assumes isotropic turbulent clustering. Unfortunately, there is no widely accepted analytical model for $E_{\mathrm{np}}(k)$. Jeffery (2000, 2001a,b) derived theoretical power spectrum models for $kl_\eta \geq 0.1$ based on a δ-correlated closure. His models, however, were obtained by assuming nonzero diffusivity of the particle number density. Recently, power spectra of the number density fluctuation have been obtained using DNS (Rani and Balachandar 2003; Shotorban and Balachandar 2007; Jin et al. 2010). For example, Jin et al. (2010) obtained the power spectra for several values of St. However, they did not discuss the Re_λ dependency or propose any model to predict the spectra. For this study, $E_{\mathrm{np}}(k)$ was calculated from the DNS data as

$$E_{\mathrm{np}}(k) = \frac{1}{\Delta k} \sum_{k-\Delta k/2 \leq |\mathbf{k}| < k+\Delta k/2} \tilde{\Phi}(\mathbf{k}), \tag{8}$$

where $\tilde{\Phi}(\mathbf{k})$ is the spectral density function of droplet number density, given by

$$\tilde{\Phi}(\mathbf{k}) = \frac{1}{L_0^3} \langle \widetilde{n_p}(\mathbf{k}) \widetilde{n_p}(-\mathbf{k}) \rangle, \tag{9}$$

where the angle brackets represent the ensemble average. The variable $\widetilde{n_p}(\mathbf{k})$ is the Fourier coefficient of the spatial droplet number density distribution $n_p(\mathbf{x})$, given by the following discrete Fourier transform

$$\widetilde{n_p}(\mathbf{k}) = \frac{1}{(2\pi)^3} \iiint_{\mathbf{x} \in V_c} n_p(\mathbf{x}) \exp(-i\mathbf{k} \cdot \mathbf{x})\, d\mathbf{x}, \tag{10}$$

where V_c is the cubic domain with edge of length $2\pi L_0$, and $n_p(\mathbf{x})$ is given by

$$n_p(\mathbf{x}) = \sum_{j=1}^{N_p} \delta(\mathbf{x} - \mathbf{x}_{p,j}), \tag{11}$$

where $\mathbf{x}_{p,j}$ is the position vector of the jth droplet inside a target domain, N_p is the total number of droplets, and $\delta(\mathbf{x})$ is the Dirac delta function. The Fourier coefficients of Eq. (11) are then given by

$$\widetilde{n_p}(\mathbf{k}) = \frac{1}{(2\pi)^3} \sum_{j=1}^{N_p} \exp(-i\mathbf{k} \cdot \mathbf{x}_{p,j}). \tag{12}$$

Note that the transform implies periodicity of the droplet distribution. Finally, substitution of Eq. (12) into Eq. (9) yields

$$\frac{\tilde{\Phi}(\mathbf{k})}{\langle n_p \rangle^2 L_0^3} = \frac{1}{N_p^2} \left\langle \sum_{j=1}^{N_p} \exp(-i\mathbf{k} \cdot \mathbf{x}_{p,j}) \sum_{j'=1, j' \neq j}^{N_p} \exp(i\mathbf{k} \cdot \mathbf{x}_{p,j'}) \right\rangle. \tag{13}$$

Note that terms for particle pairs with $j = j'$ are removed from Eq. (13) in order to eliminate white noise from $\tilde{\Phi}(\mathbf{k})$. For efficient computation of $\tilde{\Phi}(\mathbf{k})$, Eq. (13) was transformed to

$$\frac{\tilde{\Phi}(\mathbf{k})}{\langle n_p \rangle^2 L_0^3} = \left\langle \left[\frac{1}{N_p} \sum_{j=1}^{N_p} \cos(\mathbf{k} \cdot \mathbf{x}_{p,j}) \right]^2 \right\rangle + \left\langle \left[\frac{1}{N_p} \sum_{j'=1}^{N_p} \sin(\mathbf{k} \cdot \mathbf{x}_{p,j'}) \right]^2 \right\rangle - \frac{1}{N_p}. \tag{14}$$

Equation (14) still requires $N_p \times N_k$ calculations, where N_k is the number of discrete wavenumber vectors $\mathbf{k} = (m_1/L_0, m_2/L_0, m_3/L_0)$, where m_1, m_2, and m_3 are arbitrary integers. For this study, we chose 19 representative wavenumbers, giving $kL_0 = |\mathbf{k}|L_0$ values of 1, 2, 3, 4, 6, 8, 12, 16, 24, 32, 48, 64, 96, 128, 192, 256, 384, 512, and 768. These 19 values of k cover the wavenumber range more or less uniformly on a log scale. We calculated $\tilde{\Phi}(\mathbf{k})$ for the discrete wavenumbers located between the spherical surfaces with radii of $k - \Delta k/2$ and $k + \Delta k/2$, where Δk was set to $1/L_0$, and summed to calculate $E_{\rm np}(k)$ from Eq. (8). We have checked that the results are insensitive to an increased number of representative wavenumbers. The ensemble average in Eq. (14) was obtained by averaging temporal slices of the droplet distributions. For $\mathrm{Re}_\lambda \le 322$, $E_{\rm np}(k)$ was obtained by averaging 10 temporal slices, while for $\mathrm{Re}_\lambda = 531$, just a single temporal slice was used as it provided a sufficiently large data volume to obtain reliable statistics. For $\mathrm{Re}_\lambda \le 322$, the temporal slices of the droplet distributions were sampled for large intervals of $T_0 = L_0/U_0$ to eliminate the temporal correlations between the distributions.

4. Results and discussion

a. Droplet distribution in turbulence

Figure 1 shows the spatial distributions of droplets within the range $0 < z < 4l_\eta$, where $l_\eta = (\nu^3/\epsilon)^{1/4}$ is the Kolmogorov scale, for St = 0.05, 0.2, 1.0, and 5.0 at $\mathrm{Re}_\lambda = 204$. The number of the particles in each figure is similar; about 3.5×10^4. Void areas due to turbulent clustering are clearly observed for St = 1.0. For St < 1.0, the void areas are less clear. For St > 1.0, small void areas with dimensions less than $40l_\eta$ are less clear than for St = 1.0, but void areas larger than $40l_\eta$ are more prominent.

Figure 2 shows $E_{\rm np}(k)$ for St = 1.0, for different values of Re_λ. The arrow indicates the range of the nondimensional wavenumber relevant to actual radar observations, which we can estimate from the range of f_m used, and the typical l_η that apply in atmospheric clouds. The microwave frequencies used for radar observations of clouds or precipitation range from the S band ($f_m \sim 2$ GHz) to the W band ($f_m \sim 100$ GHz). The typical l_η in atmospheric clouds ranges from 5×10^{-4} to 1×10^{-3} m, which we estimate based on the energy dissipation rate $\epsilon \sim 10^{-3}$–$10^{-2}\,\mathrm{m^2\,s^{-3}}$ and $\nu \sim 10^{-5}\,\mathrm{m^2\,s^{-1}}$. Since $E_{\rm np}(k = 2k_m)$ is used for estimating $Z_{\rm cluster}$ for $f_m = k_m c_m/2\pi$, where c_m is the speed of light, the relevant wavenumber range for radar observations is estimated to be $0.05 < kl_\eta < 4.0$.

In atmospheric clouds, Re_λ ranges from 10^3 to 10^4, higher than the maximum Re_λ value (=531) used within our simulations. However, for the wavenumber range $0.05 < kl_\eta < 4.0$, the maximum difference between $E_{\rm np}(k)$ values for $\mathrm{Re}_\lambda = 204$ and 531 in Fig. 2 is 11%, while for $\mathrm{Re}_\lambda = 127$ and 531, the maximum difference is 22%. These differences correspond to differences of 0.47 and 1.1 dB in the increment to Z given by Eq. (7), respectively, where a value in units of decibels is defined as $A^{\rm dB} = 10\log_{10}A$ for a given value of A. Since errors of around 1 dB are unavoidable in radar observations (Bringi et al. 1990; Carey et al. 2000), the dependency of $E_{\rm np}(k)$ on Re_λ is sufficiently small for $\mathrm{Re}_\lambda > 200$ and thus for the wavenumber range relevant for radar observations. Thus, this study uses $E_{\rm np}(k)$ at $\mathrm{Re}_\lambda = 204$ to estimate Z for radar observations of atmospheric clouds.

Figure 3 shows $E_{\rm np}(k)$ of droplet number density fluctuations for different values of St at $\mathrm{Re}_\lambda = 204$. The horizontal and vertical axes are normalized using l_η and the average number density $\langle n_p \rangle$. It is clear that $E_{\rm np}(k)$ depends strongly on St. For St ≤ 1.0, the peak values of $E_{\rm np}(k)$ are located around $kl_\eta = 0.2$ [i.e., $(kl_\eta)_{\rm peak} \approx 0.2$] and become higher as St becomes closer to 1. This indicates that the representative void scale is almost constant, but that the number density difference between sparse (void) and dense (cluster) areas increases as St increases. This is because the number density of inertial particles tends to concentrate more in high-strain-rate and low-vorticity regions as τ_p increases (Maxey 1987). Since the Kolmogorov-scale eddies have the largest effect on the motions of St < 1 droplets, $(kl_\eta)_{\rm peak}$ is almost fixed at about 0.2. On the other hand, for St ≥ 1.0 the peak location moves toward lower wavenumbers as St increases, indicating that the representative void scale becomes larger as St increases. This is because large-scale eddies preferentially concentrate large St droplets, and small-scale eddies tend to destroy this preferential concentration by uncorrelated stirring. This scale dependent clustering mechanism is explained by Goto and Vassilicos (2006) and Yoshimoto and Goto (2007). These features for St ≤ 1.0 and St ≥ 1.0 are consistent with what is observed in Fig. 1. Jin et al. (2010) examined the St dependency of $E_{\rm np}(k)$. Their power spectra show generally good agreement with ours, confirming the reliability of our simulation. It should be noted that Jin et al. (2010) used $\mathrm{Re}_\lambda = 102$, which is too small for us to use their spectra to estimate the influence of turbulent clustering on radar observations.

b. Influence of turbulent clustering on the radar reflectivity factor

In this section the influence of turbulence on the radar reflectivity factor Z is estimated from the $E_{\rm np}(k)$ curves

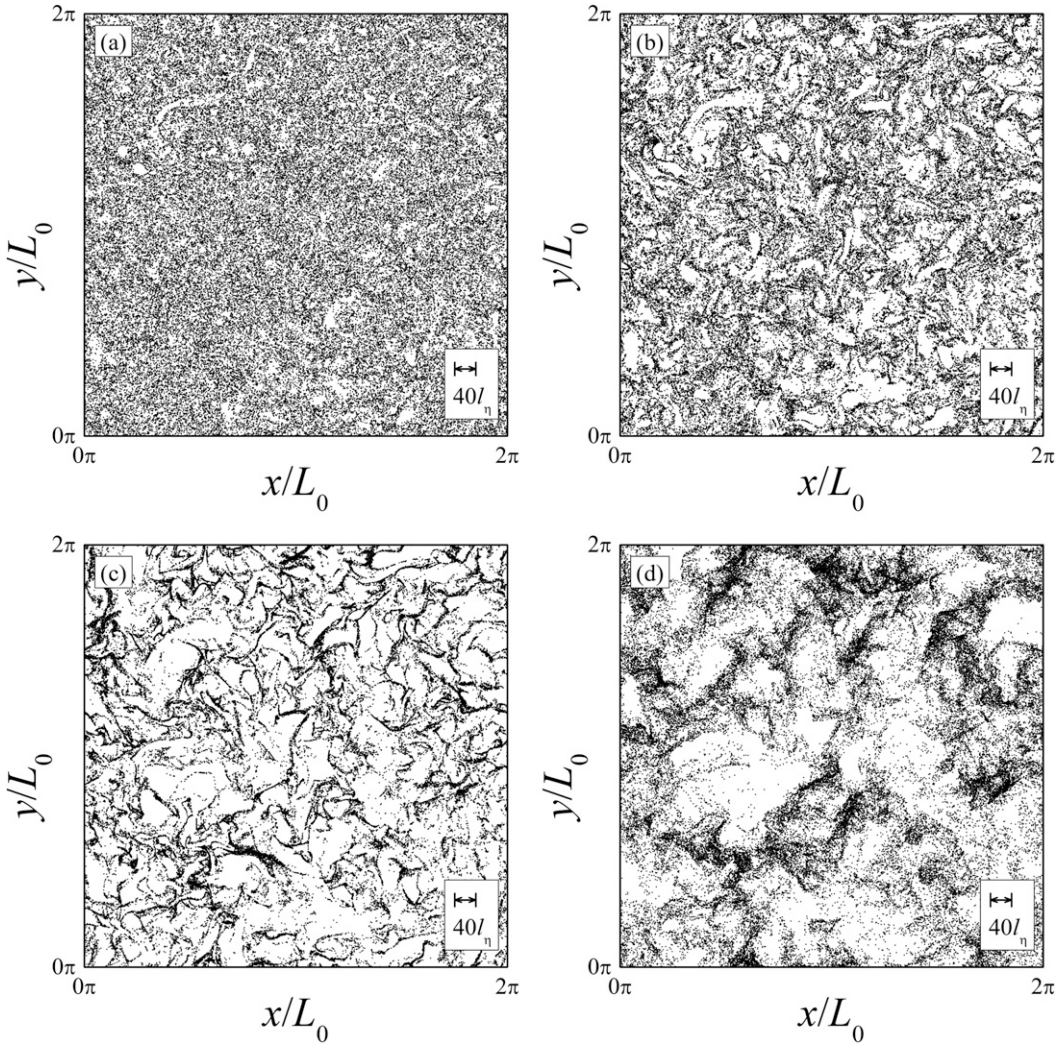

FIG. 1. Spatial distributions of droplets obtained by DNS for St = (a) 0.05, (b) 0.2, (c) 1.0, and (d) 5.0 at $\mathrm{Re}_\lambda = 204$. Only droplets in the range $0 < z < 4l_\eta$ are drawn.

shown in Fig. 3 and compared with the estimate by Dombrovsky and Zaichik (2010). The influence of turbulence is evaluated using the clustering coefficient ζ defined by

$$Z_{\text{cluster}} = (1 + \zeta) Z_{\text{random}}. \tag{15}$$

We estimate ζ from $E_{\text{np}}(k)$ using the equation

$$\zeta = \frac{2\pi^2}{\langle n_p \rangle \kappa^2} E_{\text{np}}(\kappa), \tag{16}$$

which is obtained by substituting Eqs. (6) and (7) into Eq. (15). Dombrovsky and Zaichik (2010) semianalytically estimated ζ using the following equation (Kostinski and Jameson 2000):

$$\zeta = \frac{4\pi \langle n_p \rangle}{\kappa} \int_0^\infty [g(r) - 1] r \sin(\kappa r)\, dr, \tag{17}$$

where $g(r)$ is the radial distribution function (RDF) defined as $g(r) = \langle n_p(\mathbf{x}) n_p(\mathbf{x} + \mathbf{r}) \rangle / \langle n_p \rangle^2$, where $r = |\mathbf{r}|$. [Note that Eq. (17) can be considered as the Fourier transform of Eq. (16) under isotropic conditions.] Dombrovsky and Zaichik (2010) adopted an RDF model based on the probability density function (PDF) approach (Zaichik and Alipchenkov 2007). The RDF model is

$$g(r) = c \left(\frac{r}{l_\eta} \right)^{-\Gamma}, \tag{18}$$

where the model parameters c and Γ are given by

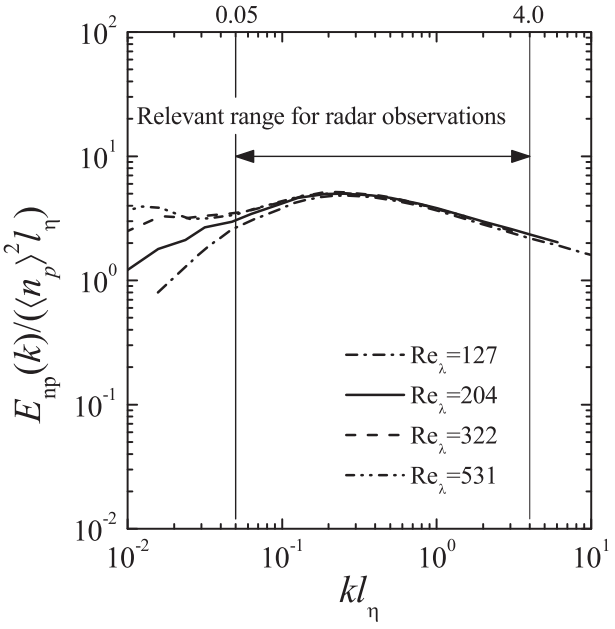

FIG. 2. Power spectra of droplet number density fluctuation obtained from DNS data for St = 1.0 at Re_λ = 127, 204, 322, and 531.

$$c = 1 + 12\mathrm{St}^2, \tag{19}$$

$$\Gamma = 6\mathrm{St}^2 - 10.4\mathrm{St}^3 + 7\mathrm{St}^4. \tag{20}$$

This RDF model is applicable to the case $\mathrm{St} < 0.6$, $\mathrm{Re}_\lambda > 30$ and $r < l_\eta$. For performing the integration from 0 to infinity in Eq. (17), Dombrovsky and Zaichik (2010) extrapolated the RDF model to the separation range $l_\eta < r < c^{1/\Gamma} l_\eta$ and assumed $g(r) - 1 = 0$ for $r > c^{1/\Gamma} l_\eta$.

Figure 4 shows clustering coefficients ζ for $\mathrm{Re}_\lambda = 204$. The horizontal axis is the microwave wavenumber difference normalized by l_η. The vertical axis is normalized by $\langle n_p\rangle l_\eta^3$ to eliminate the effect of droplet number density. The horizontal arrow indicates the typical range of the nondimensional wavenumber in actual radar observations; $0.05 < \kappa l_\eta < 4.0$, corresponding to the arrow in Fig. 2. In this wavenumber range, the ζ values obtained from the $E_{\mathrm{np}}(k)$ data show a strong dependency on St and a monotonically decreasing trend against kl_η. The St dependency was also analyzed in Dombrovsky and Zaichik (2010). However, they did not find the monotonically decreasing trends seen in our results: the ζ values of Dombrovsky and Zaichik (2010) are almost constant in the low-wavenumber region and decrease with wavy oscillations as the wavenumber increases. These two characteristics exist because the extrapolation of their RDF model to $r > l_\eta$ is physically unrealistic, and the RDF for $r > l_\eta$ has a large influence on ζ. Since the number density correlation function

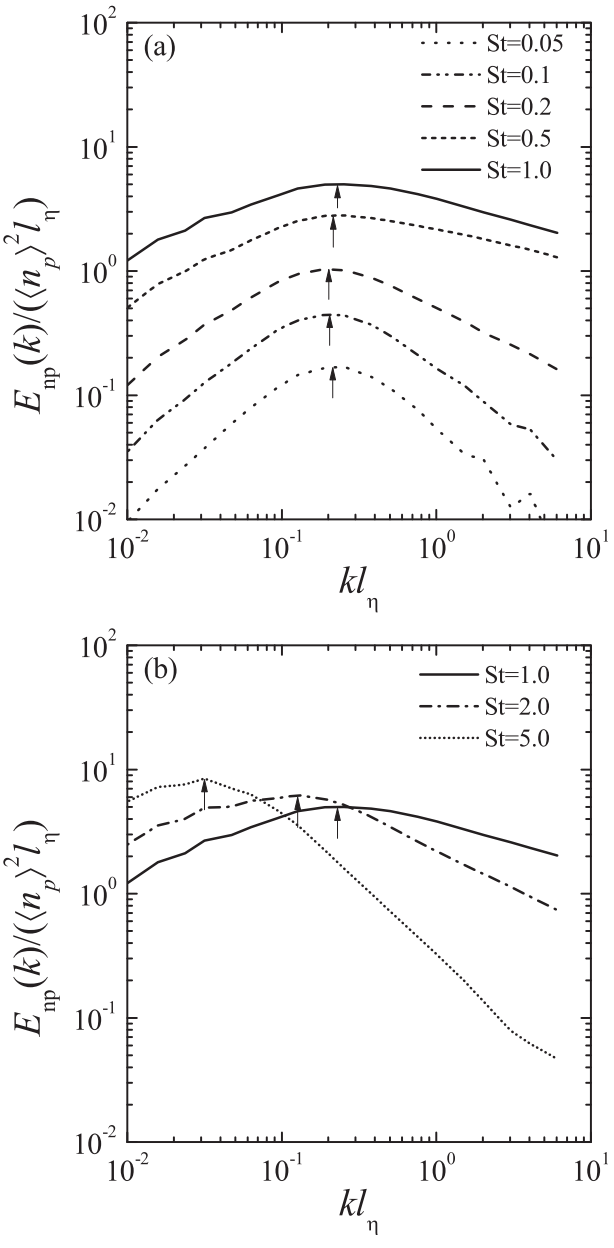

FIG. 3. Power spectra of droplet number density fluctuation obtained from DNS data for (a) $\mathrm{St} \le 1$ and (b) $\mathrm{St} \ge 1$ at $\mathrm{Re}_\lambda = 204$. The small arrows indicate the peak location of each spectrum.

$\langle n_p(\mathbf{x}) n_p(\mathbf{x}+\mathbf{r})\rangle$ for $r > l_\eta$ is considered in the calculation of $E_{\mathrm{np}}(k)$, the estimate of ζ based on $E_{\mathrm{np}}(k)$ is more reliable than that based on their RDF model.

c. *Modeling of the turbulent clustering influence on radar reflectivity factor*

In this section we develop a new empirical model of the radar reflectivity factor as a function of kl_η and St by fitting curves to those of $E_{\mathrm{np}}(k)$ in Fig. 3. The $E_{\mathrm{np}}(k)$ curves in Fig. 3 show power-law-like slopes for $kl_\eta < (kl_\eta)_{\mathrm{peak}}$

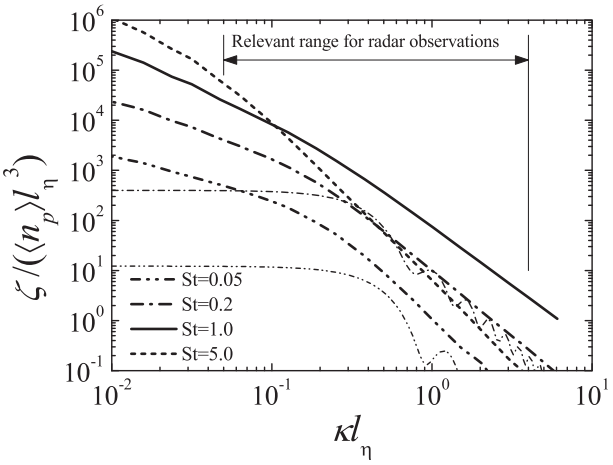

FIG. 4. Clustering coefficients obtained from the $E_{np}(k)$ data for $Re_\lambda = 204$ shown in Fig. 3 (thick lines) and those estimated by Dombrovsky and Zaichik (2010) (thin lines), which are only applicable for $St < 0.6$.

and $kl_\eta > (kl_\eta)_{peak}$, so we assume that the power spectra of number density fluctuations asymptotically approach $E_{np}(k)/(\langle n_p\rangle^2 l_\eta) \approx c_1(kl_\eta)^\alpha$ and $E_{np}(k)/(\langle n_p\rangle^2 l_\eta) \approx c_1(kl_\eta)^\beta$ in the small- and large-wavenumber regions, respectively. For intermediate wavenumbers, we connect the two asymptotic regimes with a function based on the power spectrum model of scalar concentration fluctuations suggested by Hill (1978) (model 2). That is, we assume

$$\frac{d\ln S(\xi)}{d\xi^\dagger} = \frac{\alpha}{2}[1-\tanh(\gamma\xi^\dagger)] + \frac{\beta}{2}[1+\tanh(\gamma\xi^\dagger)], \quad (21)$$

where $S(\xi)$ is the nondimensional spectrum defined as $S(\xi) = S(kl_\eta) = E_{np,model}(k)/(\langle n_p\rangle^2 l_\eta)$, ξ is the nondimensional wavenumber defined as $\xi = kl_\eta$, and γ is a positive-valued parameter enabling us to adjust the peak value in the transition region. The term $\xi^\dagger$ is defined as $\xi^\dagger = \ln(\xi/\xi_t)$, where ξ_t is the nondimensional transition wavenumber. Under the conditions $S(\xi) \to c_1\xi^\alpha$ for $\xi \to 0$ and $S(\xi) \to c_2\xi^\beta$ for $\xi \to \infty$, ξ_t becomes $(c_2/c_1)^{1/(\alpha-\beta)}$ so that $S(\xi)$ becomes

$$S(\xi) = \frac{c_1\xi^\alpha}{[1+(c_1/c_2)^{2\gamma/(\alpha-\beta)}\xi^{2\gamma}]^{(\alpha-\beta)/2\gamma}}. \quad (22)$$

Figure 5 shows the values of the parameters c_1, α, c_2, and β for each of the Stokes numbers. The parameters c_1 and α were obtained by finding a least squares fit within the wavenumber range $kl_\eta < 0.1$, while c_2 and β were obtained by finding the best fit for $kl_\eta > 0.7$. The solid lines are the best-fit curves, given by

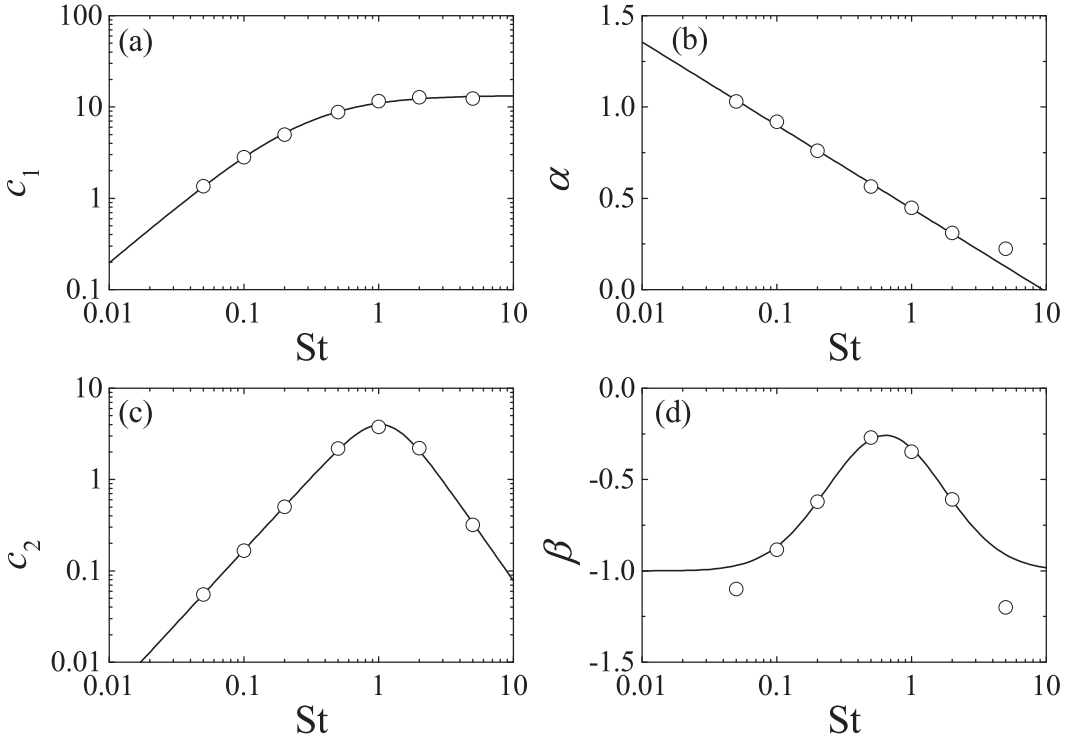

FIG. 5. Model parameters in Eq. (22) vs the Stokes number: (a) c_1, (b) α, (c) c_2, and (d) β. The solid lines show the best-fit curves given by Eqs. (23) and (24).

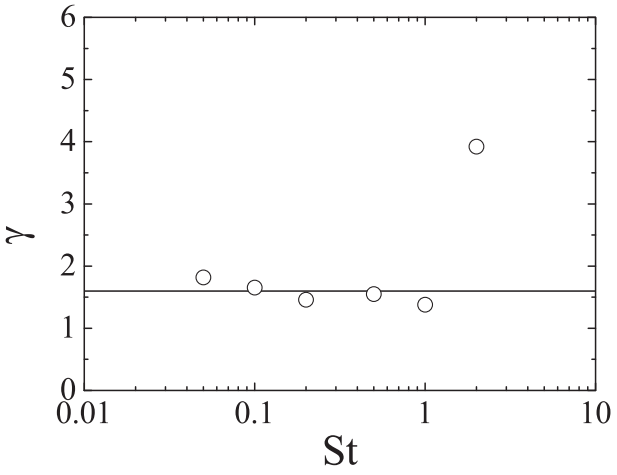

FIG. 6. Model parameter γ in Eq. (22) vs the Stokes number. The solid line shows the average γ value (1.6) obtained when the rightmost point is excluded.

$$\begin{cases} c_1 = 13.4/[1 + (\mathrm{St}/0.29)^{-1.25}], \\ \alpha = 0.44 - 0.20 \ln \mathrm{St}, \end{cases} \tag{23}$$

and

$$\begin{cases} c_2 = 6.7\mathrm{St}^{1.6}/(1 + 0.68\mathrm{St}^{3.7}), \\ \beta = -1 + 0.77\mathrm{St}^{-1} \exp\{-[\ln(\mathrm{St}) - 0.55]^2/2.0\}. \end{cases} \tag{24}$$

Note that the reference data for c_1 and α for St = 5.0 were fewer and less reliable than those for the other St values. This is because the peak of $E_{\mathrm{np}}(k)$ is located in the region $kl_\eta < 0.1$. Thus, the α value for St = 5.0 was not considered in obtaining Eq. (23). Since the diffusion coefficient of the droplet number density is much smaller than ν, the value of β for St $\ll 1$ should be -1, which is the power index of the power spectrum of scalar concentration fluctuation in the viscous-convective range (Batchelor 1959; Grant et al. 1968; Goto and Kida 1999). The behavior of β for St $\gg 1$ is unknown. For this study, we simply assume that β approaches -1 for St $\gg 1$. This simple assumption affects only large St values, where the influence of turbulence is negligibly small in radar observations (as will be seen in Fig. 9, described in section 4e).

Figure 6 shows the parameter γ which appears in Eq. (22). We see that γ is nearly constant for St ≤ 1.0 but becomes larger for St > 1.0. For this study we have ignored the γ values for St > 1.0 and averaged those for St ≤ 1.0, giving

$$\gamma = 1.6. \tag{25}$$

This is justified by the fact that adjustment of γ for St $>$ 1.0 resulted in only small improvements to the fit.

To summarize, our model of the influence of the microscale turbulent clustering $S(\xi)$ is estimated from Eq. (22) together with Eqs. (23)–(25). The clustering coefficient (i.e., the increment due to turbulent clustering) is then obtained from Eq. (16) as

$$\frac{\zeta}{\langle n_p \rangle l_\eta^3} = \frac{2\pi^2}{(\kappa l_\eta)^2} S(\kappa l_\eta), \tag{26}$$

where $\kappa = 2k_m$.

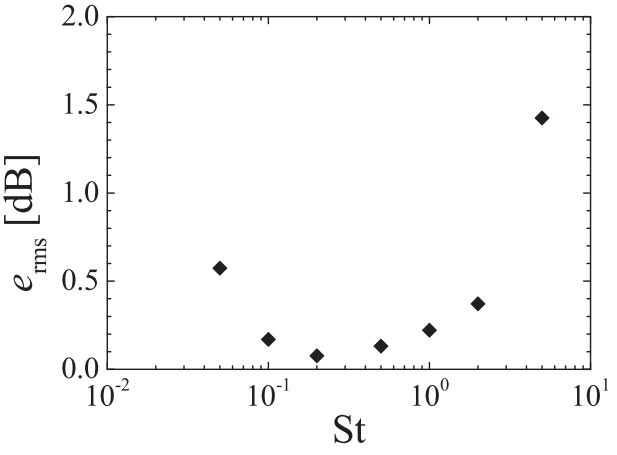

FIG. 7. RMS error of the proposed power spectrum model $E_{\mathrm{np,model}}(k)$. The error is evaluated within the wavenumber range relevant for radar observations: $0.05 < kl_\eta < 4.0$.

Figure 7 shows the RMS error e_{rms} of the proposed model $E_{\mathrm{np,model}}(k)$, evaluated in units of decibels, in which e_{rms} is calculated for the wavenumber range relevant for radar observations—$0.05 < kl_\eta < 4.0$—using the equation

$$e_{\mathrm{rms}} = \left\{ \frac{1}{\xi'_{\max} - \xi'_{\min}} \times \int_{\xi'_{\min}}^{\xi'_{\max}} [E_{\mathrm{np}}^{\mathrm{dB}}(k) - E_{\mathrm{np,model}}^{\mathrm{dB}}(k)]^2 \, d\xi' \right\}^{1/2}, \tag{27}$$

where the superscript dB denotes a value in units of decibels, ξ' is defined as $\xi' = \ln(kl_\eta)$, and $\xi'_{\min}$ and $\xi'_{\max}$ are set to ln(0.05) and ln(4.0), respectively. Also e_{rms} has its minimum value at St = 0.2. For St < 0.2, for which turbulent clustering is less pronounced than for St > 0.2, the increase of e_{rms} as St reduces is due to an increase of statistical error in the reference $E_{\mathrm{np}}(k)$ data, which is observed as fluctuations of $E_{\mathrm{np}}(k)$ for St = 0.05 and 0.1 and $kl_\eta > 1$ in Fig. 3. In the range St > 0.2, we see significant increases in error from St = 2.0, mainly caused by the simple assumptions for β when St $\gg 1$. However, as will be discussed later in section 4e, the clustering effect for St ≥ 5.0 is irrelevant for actual radar observations. Except for St = 5.0, e_{rms} is well below 1 dB. As mentioned in section 4a, we consider this level of error to be acceptable.

TABLE 2. Numerical conditions for the cases with gravity included: S_v is the nondimensional terminal velocity defined by $S_v = v_T/u_\eta$ and Fr is the Froude number defined by $\mathrm{Fr} = v_T/u_{\mathrm{rms}}$. Re_λ and St were set to 204 and 1.0, respectively.

S_v	Fr	g (m s^{-2})
0.00	0.00	0.0
1.36	0.188	9.8
2.68	0.369	9.8
6.79	0.936	9.8
11.0	1.51	9.8

d. *Influence of gravitational settling on the power spectra of number density fluctuations*

The influence of gravitational settling on the power spectra of number density fluctuations has been investigated by performing additional DNSs with gravity included. Nondimensional parameters relevant for gravitational effects are $S_v = v_T/u_\eta$—where v_T is the terminal velocity given by $\tau_p g$ and u_η is the Kolmogorov velocity (Wang and Maxey 1993; Grabowski and Vaillancourt 1999)—and the Froude number ($\mathrm{Fr} = v_T/u_{\mathrm{rms}}$); S_v measures the settling influence on small scales and Fr measures it on large scales. Strictly speaking, we need multiple parameters covering the wide range of clustering scales. However, we consider these two parameters—covering the two ends of the scale range—to be sufficient for our analysis. Table 2 shows the values of S_v and Fr in the additional DNS runs. Re_λ was set to 204 and St to unity.

Figure 8 shows the settling influence on $E_{\mathrm{np}}(k)$. As the particle settling becomes stronger, $E_{\mathrm{np}}(k)$ decreases at small scales and increases at large scales. The decrease at small scales corresponds to the increase of S_v and indicates that settling weakens small-scale clustering (Ayala et al. 2008a,b; Woittiez et al. 2009). The increase at large scales, on the other hand, corresponds to the increase of Fr and indicates that anisotropies generated by settling lead to large-scale clustering. [Woittiez et al. (2009) observed a nearly-two-dimensional "curtain shape" clustering.] However, the increase at large scales is outside of the wavenumber range relevant for radar observations, so we need only consider S_v. The maximum differences between $E_{\mathrm{np}}(k)$ for $S_v > 0$ and $S_v = 0$ are 0.35, 0.68, 1.4, and 2.2 dB for $S_v = 1.37$, 2.71, 6.88, and 11.1, respectively. That is, the errors of the proposed model are smaller than 1 dB for $S_v \leq 2.7 \approx 3$. Thus the proposed model is reliable for $S_v < 3$.

e. *Turbulent clustering influence in radar observations estimated by the proposed model*

Recent radar observations of clouds and precipitation have been conducted using microwaves in six frequency bands: the S, C, X, Ku, Ka, and W bands, with typically used frequencies of 2.8, 5.3, 9.4, 13.8, 35, and 94 GHz,

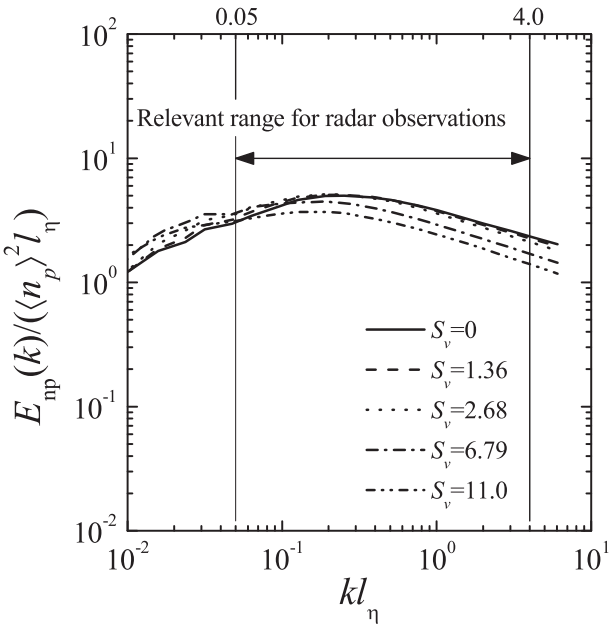

FIG. 8. Influence of gravitational settling on the power spectra of droplet number density fluctuation for St = 1.0 at $\mathrm{Re}_\lambda = 204$.

respectively. The S-, C-, X-, and Ku-band radars are often used for observing precipitation, while Ka- and W-band radars are used only for clouds. This is because the Rayleigh scattering approximation is invalid when d_p/λ_m is larger than about 1/10, where d_p is the droplet diameter and λ_m the microwave wavelength. That is, the Rayleigh scattering approximation is invalid for r_p larger than 430 and 160 μm for the Ka and W bands, respectively. The S and X bands are also used for cloud observations, often using dual frequencies to retrieve liquid water content (LWC)—the liquid water mass contained in a unit volume of air. In dual-wavelength radar observations, LWC is estimated from the dual-wavelength ratio (DWR), which is defined as the difference of Z^{dB} (dBZ) [$=10\log_{10}Z$ (mm^6 m^{-3})] for two frequencies (Knight and Miller 1998; Vivekanandan et al. 1999; Wang et al. 2005; Ellis and Vivekanandan 2011) and analyzed by considering the frequency dependency of microwave attenuation. To take a recent example, Ellis and Vivekanandan (2011) proposed and tested a technique for estimating cloud LWC using the National Center for Atmospheric Research (NCAR) simultaneous S-band–Ka-band dual-polarimetric (S-PolKa) radar system.

We now estimate increments to Z^{dB} due to microscale turbulent clustering [i.e., $Z^{\mathrm{dB}}_{\mathrm{cluster}} - Z^{\mathrm{dB}}_{\mathrm{random}} = (1+\zeta)^{\mathrm{dB}}$] under two idealized cloud scenarios: (i) a stratocumulus case, where $l_\eta = 1 \times 10^{-3}$ m and thus $\epsilon \approx 3 \times 10^{-3}$ m^2 s^{-3}, and (ii) a cumulus case, where $l_\eta = 5 \times 10^{-4}$ m and thus $\epsilon \approx 5 \times 10^{-2}$ m^2 s^{-3} (Pinsky et al. 2008). For both cases,

the volume fraction was kept at $\phi = 10^{-6}$. For simplicity, the cloud droplets are assumed to be monodispersed, though in real clouds, droplets have various kinds of size distribution. Since ϕ is fixed to a constant value, $\langle n_p \rangle$ varies depending on the droplet size as follows:

$$\langle n_p \rangle l_\eta^3 = \frac{3\phi}{4\pi}\left(\frac{r_p}{l_\eta}\right)^{-3}, \tag{28}$$

where $r_p/l_\eta = \sqrt{(9/2)(\rho_a/\rho_p)\mathrm{St}}$ and $\rho_p/\rho_a = 840$. For atmospheric clouds, ϕ is in the range $10^{-7} < \phi < 10^{-6}$ (Kokhanovsky 2004), so the chosen condition $\phi = 10^{-6}$ corresponds to dense clouds.

It should be noted that turbulent entrainment can also be a cause of droplet number density fluctuations in real clouds. However, we can separate the influence of turbulent entrainment from that of turbulent clustering by using the well-known scalar concentration spectrum $E_\theta(k)$. In the inertial-convective range ($kl_\eta < 0.1$), $E_\theta(k)$ is given by

$$\frac{E_\theta(k)}{\chi\epsilon^{-3/4}\nu^{5/4}} = C_c(kl_\eta)^{-5/3}, \tag{29}$$

where χ is the scalar dissipation rate and C_c is the Obukhov–Corrsin constant (Sreenivasan 1996; Goto and Kida 1999). In the viscous-convective range ($kl_\eta > 0.1$), $E_\theta(k)$ is given by

$$\frac{E_\theta(k)}{\chi\epsilon^{-3/4}\nu^{5/4}} = C_b(kl_\eta)^{-1}, \tag{30}$$

where C_b is the Batchelor constant (Batchelor 1959; Grant et al. 1968; Oakey 1982; Goto and Kida 1999). Note that Eq. (30) is valid when the scalar diffusive coefficient D is much smaller than ν. Since the scales of clustering and entrainment are typically well separated, the correlation between the number density fluctuations due to clustering and entrainment should be negligible. Thus, $E_{\mathrm{np}}(k)$ for both clustering and entrainment should be given by $E_{\mathrm{np}}(k) = E_{\mathrm{np}}^{\mathrm{clust}}(k) + E_{\mathrm{np}}^{\mathrm{entr}}(k)$, where $E_{\mathrm{np}}^{\mathrm{clust}}(k)$ and $E_{\mathrm{np}}^{\mathrm{entr}}(k)$ are the power spectra for clustering and entrainment, respectively. Here we focus on the influence of $E_{\mathrm{np}}^{\mathrm{clust}}(k)$.

Figure 9 shows values of $Z_{\mathrm{cluster}}^{\mathrm{dB}} - Z_{\mathrm{random}}^{\mathrm{dB}}$ estimated from the proposed model together with the DNS results. For r_p smaller than 100 μm, the increment $Z_{\mathrm{cluster}}^{\mathrm{dB}} - Z_{\mathrm{random}}^{\mathrm{dB}}$ for each value of f_m is larger in the cumulus case than in the stratocumulus case. The increment is larger than the observation error level (1 dB) for $f_m \leq 9.4$ GHz in the stratocumulus case and for $f_m \leq 13.8$ GHz in the cumulus case. However, the influence is not significant for larger drops. This is because, for St > 1, $E_{\mathrm{np}}(k)/(\langle n_p \rangle^2 l_\eta)$ becomes smaller as St increases, and $\langle n_p \rangle$ decreases as

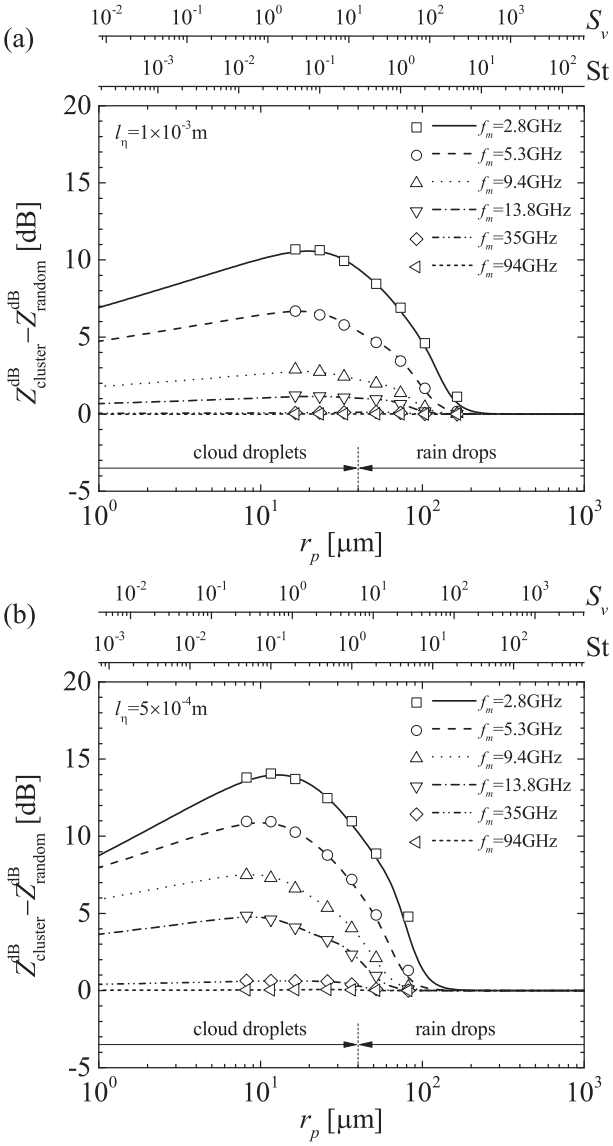

FIG. 9. Influence of turbulent clustering on the radar reflectivity factor (i.e., $Z_{\mathrm{cluster}}^{\mathrm{dB}} - Z_{\mathrm{random}}^{\mathrm{dB}}$), estimated from our proposed model (lines) and the DNS results (symbols) as a function of droplet radius in (a) a stratocumulus case, where $l_\eta = 1 \times 10^{-3}$ m, and (b) a strong cumulus case, where $l_\eta = 5 \times 10^{-4}$ m. The values $f_m = 2.8$, 5.3, 9.4, 13.8, 35, and 94 GHz are typically used radar frequencies in the S, C, X, Ku, Ka, and W bands, respectively.

r_p increases, as indicated in Eq. (28). The peak of $Z_{\mathrm{cluster}}^{\mathrm{dB}} - Z_{\mathrm{random}}^{\mathrm{dB}}$ for each f_m is located at St ≈ 0.1, which corresponds to droplet radii of a few tens of micrometers—close to the typical cloud droplet size. Thus, the influence of turbulence can cause a significant error in retrieving the LWC of clouds in radar observations with microwave frequencies less than 13.8 GHz (S, C, X, and Ku bands).

For $S_v > 3$ however, the influence of turbulent clustering would be overestimated significantly owing to the

influence of gravitational settling, as discussed in section 4d. The threshold $S_v = 3$ corresponds to $r_p \approx 20\,\mu$m for the stratocumulus case and to $r_p \approx 30\,\mu$m for the cumulus case. The possible overestimates for large r_p cannot be ignored, but they do not affect our main argument that the influence of turbulence can cause a significant error in radar observations using the S, C, X, and Ku bands.

Figure 9 indicates that the radar reflectivity factor becomes larger as f_m becomes lower and that the maximum difference between the S and X bands is approximately 8 dB. These characteristics are in good agreement with the observations of developing cumulus clouds by Knight and Miller (1998), in which the reflectivity factor for the S band is about 10 dB larger than for the X band. As mentioned in the introduction, a similar frequency dependency was found for the case of smoke plumes of an industrial fire by Rogers and Brown (1997). Although the constituents and sizes of smoke particles are different from cloud droplets, turbulence could also influence the radar reflectivity factor. Thus, as speculated by Kostinski and Jameson (2000) based on the theory of particulate Bragg scattering, turbulent clustering may influence the radar observation of cumulus clouds and smoke plumes.

5. Conclusions

This study has investigated the influence of microscale turbulent clustering of cloud droplets on the radar reflectivity factor and proposed an empirical parameterization to account for it. Three-dimensional direct numerical simulations (DNS) of particle-laden isotropic turbulence were performed in order to obtain turbulent clustering data, from which power spectra of droplet number density fluctuations were calculated. The calculated power spectra show dependencies on the Taylor microscale-based Reynolds number (Re_λ) and the Stokes number (St). To begin, we investigated the dependency of the turbulent clustering influence on Re_λ. Results for a wide range of Re_λ values (up to 531) reveal that $\mathrm{Re}_\lambda = 204$ is large enough to be representative of the whole wavenumber range relevant to radar observations of atmospheric clouds ($0.05 < kl_\eta < 4$, where k is the wavenumber and l_η is the Kolmogorov scale). (Smaller Re_λ values were found to be unable to represent the power spectrum for low wavenumbers.) Setting $\mathrm{Re}_\lambda = 204$, we then investigated the dependency on St. We observed that for $\mathrm{St} < 1$ the peak of the power spectrum is located at around $kl_\eta = 0.2$ with the peak value increasing as the Stokes number increases toward unity. For $\mathrm{St} > 1$, the peak location moves to lower wavenumbers as St increases. Based on these observations, and assuming that the power spectrum follows distinct power laws in the small- and large-wavenumber regions, we proposed an empirical model that approximately fits the power spectrum of number density fluctuations $E_{\mathrm{np}}(k)$. From this model, it was then possible to calculate the clustering coefficient ζ (i.e., the influence of turbulence on the radar reflectivity factor). A comparison between the model estimates and the DNS results for $E_{\mathrm{np}}(k)$ confirms the reliability of the model for droplets with Stokes number smaller than 2. For larger Stokes number droplets, the model estimate has larger errors, but the influence of turbulence of such large droplets is likely negligible in typical clouds. The proposed model has been applied to two idealized radar-observation scenarios: (i) a stratocumulus case, where $l_\eta = 1 \times 10^{-3}$ m, and (ii) a cumulus case, where $l_\eta = 5 \times 10^{-4}$ m. In both cases, the droplet volume fraction was 10^{-6} and the microwave frequency f_m ranged from 2.8 to 94 GHz. The results show that the influence of microscale turbulent clustering on the radar reflectivity factor is significant for droplets with radius smaller than 100 μm for $f_m \leq 9.4$ GHz in the stratocumulus case and for $f_m \leq 13.8$ GHz in the cumulus case. That is, the influence of turbulent clustering can cause a significant error in retrieving cloud liquid water content from radar observations with microwave frequencies less than 13.8 GHz (S, C, X, and Ku bands). Additional DNSs with gravitational effects included reveal that the influence of gravitational settling causes significant errors in the model estimates when the nondimensional terminal velocity S_v is larger than 3. These errors for large particles cannot be ignored but do not alter our main conclusions.

Acknowledgments. The authors thank Dr. Masaki Katsumata of the Japan Agency for Marine-Earth Science and Technology for his helpful comments on radar observations. The numerical simulations presented here were carried out on the Earth Simulator 2 and ICE X supercomputer systems operated by the Japan Agency for Marine-Earth Science and Technology. This study was supported by Grant-in-Aid for Young Scientists (A) (20686015) and by Grant-in-Aid for JSPS Fellows (21·241).

REFERENCES

Ayala, O., B. Rosa, L.-P. Wang, and W. Grabowski, 2008a: Effects of turbulence on the geometric collision rate of sedimenting droplets. Part 1. Results from direct numerical simulation. *New J. Phys.,* **10,** 075015, doi:10.1088/1367-2630/10/7/075015.

——, ——, and ——, 2008b: Effects of turbulence on the geometric collision rate of sedimenting droplets. Part 2. Theory and parameterization. *New J. Phys.,* **10,** 075016, doi:10.1088/1367-2630/10/7/075016.

Batchelor, G., 1959: Small-scale variation of convected quantities like temperature in turbulent fluid Part 1. General discussion

and the case of small conductivity. *J. Fluid Mech.,* **5,** 113–133, doi:10.1017/S002211205900009X.

Bohren, C., and D. Huffman, 1983: *Absorption and Scattering of Light by Small Particles.* Wiley, 530 pp.

Bringi, V., V. Chandrasekar, N. Balakrishnan, and D. Zrnić, 1990: An examination of propagation effects in rainfall on radar measurements at microwave frequencies. *J. Atmos. Oceanic Technol.,* **7,** 829–840, doi:10.1175/1520-0426(1990)007<0829:AEOPEI>2.0.CO;2.

Carey, L. D., S. A. Rutledge, D. A. Ahijevych, and T. D. Keenan, 2000: Correcting propagation effects in C-band polarimetric radar observations of tropical convection using differential propagation phase. *J. Atmos. Sci.,* **39,** 1405–1433, doi:10.1175/1520-0450(2000)039<1405:CPEICB>2.0.CO;2.

Chen, L., S. Goto, and J. Vassilicos, 2006: Turbulent clustering of stagnation points and inertial particles. *J. Fluid Mech.,* **553,** 143–154, doi:10.1017/S0022112006009177.

Dombrovsky, L., and L. Zaichik, 2010: An effect of turbulent clustering on scattering of microwave radiation by small particles in the atmosphere. *J. Quant. Spectrosc. Radiat. Transfer,* **111,** 234–242, doi:10.1016/j.jqsrt.2009.09.003.

Ellis, S., and J. Vivekanandan, 2011: Liquid water content estimates using simultaneous s and k_a band radar measurements. *Radio Sci.,* **46,** RS2021, doi:10.1029/2010RS004361.

Erkelens, J., V. Venema, H. Russchenberg, and L. Ligthart, 2001: Coherent scattering of microwave by particles: Evidence from clouds and smoke. *J. Atmos. Sci.,* **58,** 1091–1102, doi:10.1175/1520-0469(2001)058<1091:CSOMBP>2.0.CO;2.

Gossard, E. E., and R. G. Strauch, 1983: *Radar Observation of Clear Air and Clouds.* Developments in Atmospheric Science, Vol. 14, Elsevier, 292 pp.

Goto, S., and S. Kida, 1999: Passive scalar spectrum in isotropic turbulence: Prediction by the Lagrangian direct-interaction approximation. *Phys. Fluids,* **11,** 1936–1952, doi:10.1063/1.870055.

——, and J. C. Vassilicos, 2006: Self-similar clustering of inertial particles and zero-acceleration points in fully developed two-dimensional turbulence. *Phys. Fluids,* **18,** 115103, doi:10.1063/1.2364263.

Grabowski, W., and P. Vaillancourt, 1999: Comments on ''Preferential concentration of cloud droplets by turbulence: Effects on the early evolution of cumulus cloud droplet spectra.'' *J. Atmos. Sci.,* **56,** 1433–1436, doi:10.1175/1520-0469(1999)056<1433:COPCOC>2.0.CO;2.

Grant, H., B. Hughes, W. Vogel, and A. Moilliet, 1968: The spectrum of temperature fluctuations in turbulent flow. *J. Fluid Mech.,* **34,** 423–442, doi:10.1017/S0022112068001990.

Hill, R., 1978: Models of the scalar spectrum for turbulent advection. *J. Fluid Mech.,* **88,** 541–562, doi:10.1017/S002211207800227X.

Hirt, C., and J. Cook, 1972: Calculating three-dimensional flow around structures. *J. Comput. Phys.,* **10,** 324–340, doi:10.1016/0021-9991(72)90070-8.

Jeffery, C. A., 2000: Effect of particle inertia on the viscous-convective subrange. *Phys. Rev.,* **61E,** 6578–6585, doi:10.1103/PhysRevE.61.6578.

——, 2001a: Investigating the small-scale structure of clouds using the δ-correlated closure: Effect of particle inertia, condensation/evaporation and intermittency. *Atmos. Res.,* **59–60,** 199–215, doi:10.1016/S0169-8095(01)00116-8.

——, 2001b: Statistical models of cloud-turbulence interactions. M.S. thesis, Dept. of Earth and Ocean Sciences, The University of British Columbia, 122 pp.

Jin, G., G.-W. He, and L.-P. Wang, 2010: Large-eddy simulation of turbulent collision of heavy particles in isotropic turbulence. *Phys. Fluids,* **22,** 055106, doi:10.1063/1.3425627.

Kim, I., S. Elghobashi, and W. Sirignano, 1998: On the equation for spherical-particle motion: Effect of Reynolds and acceleration numbers. *J. Fluid Mech.,* **367,** 221–253, doi:10.1017/S0022112098001657.

Knight, C., and L. Miller, 1993: First radar echoes from cumulus clouds. *Bull. Amer. Meteor. Soc.,* **74,** 179–188, doi:10.1175/1520-0477(1993)074<0179:FREFCC>2.0.CO;2.

——, and ——, 1998: Early radar echoes from small, warm cumulus: Bragg and hydrometeor scattering. *J. Atmos. Sci.,* **55,** 2974–2992, doi:10.1175/1520-0469(1998)055<2974:EREFSW>2.0.CO;2.

Kokhanovsky, A., 2004: Optical properties of terrestrial clouds. *Earth-Sci. Rev.,* **64,** 189–241, doi:10.1016/S0012-8252(03)00042-4.

Kostinski, A., and A. Jameson, 2000: On the spatial distribution of cloud particles. *J. Atmos. Sci.,* **57,** 901–915, doi:10.1175/1520-0469(2000)057<0901:OTSDOC>2.0.CO;2.

Matsuda, K., R. Onishi, R. Kurose, and S. Komori, 2012: Turbulence effect on cloud radiation. *Phys. Rev. Lett.,* **108,** 224502, doi:10.1103/PhysRevLett.108.224502.

Maxey, M., 1987: The gravitational settling of aerosol particles in homogeneous turbulence and random flow fields. *J. Fluid Mech.,* **174,** 441–465, doi:10.1017/S0022112087000193.

——, and J. Riley, 1983: Flow due to an oscillating sphere and an expression for unsteady drag on the sphere at finite Reynolds number. *Phys. Fluids,* **26,** 883–889, doi:10.1063/1.864230.

Morinishi, Y., T. Lundm, O. Vasilyev, and P. Moin, 1998: Fully conservative higher order finite difference schemes for incompressible flow. *J. Comput. Phys.,* **143,** 90–124, doi:10.1006/jcph.1998.5962.

Oakey, N., 1982: Determination of the rate of dissipation of turbulent energy from simultaneous temperature and velocity shear microstructure measurements. *J. Phys. Oceanogr.,* **12,** 256–271, doi:10.1175/1520-0485(1982)012<0256:DOTROD>2.0.CO;2.

Okamoto, H., and Coauthors, 2007: Vertical cloud structure observed from shipborne radar and lidar: Midlatitude case study during the MR01/K02 cruise of the research vessel Mirai. *J. Geophys. Res.,* **112,** D08216, doi:10.1029/2006JD007628.

Onishi, R., and J. Vassilicos, 2014: Collision statistics of inertial particles in two-dimensional homogeneous isotropic turbulence with an inverse cascade. *J. Fluid Mech.,* **745,** 279–299, doi:10.1017/jfm.2014.97.

——, K. Takahashi, and S. Komori, 2009: Influence of gravity on collisions of monodispersed droplets in homogeneous isotropic turbulence. *Phys. Fluids,* **21,** 125108, doi:10.1063/1.3276906.

——, Y. Baba, and K. Takahashi, 2011: Large-scale forcing with less communication in finite-difference simulations of steady isotropic turbulence. *J. Comput. Phys.,* **230,** 4088–4099, doi:10.1016/j.jcp.2011.02.034.

——, K. Takahashi, and J. Vassilicos, 2013: An efficient parallel simulation of interacting inertial particles in homogeneous isotropic turbulence. *J. Comput. Phys.,* **242,** 809–827, doi:10.1016/j.jcp.2013.02.027.

Pinsky, M., and A. Khain, 1997: Turbulence effect on droplet growth and size distribution in clouds—A review. *J. Aerosol Sci.,* **28,** 1177–1214, doi:10.1016/S0021-8502(97)00005-0.

——, ——, and H. Krugliak, 2008: Collision of cloud droplets in a turbulent flow. Part V: Application of detailed tables of turbulent collision rate enhancement to simulation of droplet spectra evolution. *J. Atmos. Sci.,* **65,** 357–374, doi:10.1175/2007JAS2358.1.

Rani, S., and S. Balachandar, 2003: Evaluation of the equilibrium Eulerian approach for the evolution of particle concentration in isotropic turbulence. *Int. J. Multiphase Flow,* **29,** 1793–1816, doi:10.1016/j.ijmultiphaseflow.2003.09.005.

Reade, W., and L. Collins, 2000: Effect of preferential concentration on turbulent collision rates. *Phys. Fluids,* **12,** 2530, doi:10.1063/1.1288515.

Rogers, R., and W. Brown, 1997: Radar observations of a major industrial fire. *Bull. Amer. Meteor. Soc.,* **78,** 803–814, doi:10.1175/1520-0477(1997)078<0803:ROOAMI>2.0.CO;2.

Shotorban, B., and S. Balachandar, 2007: A Eulerian model for large-eddy simulation of concentration of particles with small Stokes numbers. *Phys. Fluids,* **19,** 118107, doi:10.1063/1.2804956.

Squires, K., and J. Eaton, 1991: Preferential concentration of particles by turbulence. *Phys. Fluids,* **3A,** 1169–1178, doi:10.1063/1.858045.

Sreenivasan, K., 1996: The passive scalar spectrum and the Obukhov-Corrsin constant. *Phys. Fluids,* **8,** 189–196, doi:10.1063/1.868826.

Stephens, G., and Coauthors, 2008: CloudSat mission: Performance and early science after the first year of operation. *J. Geophys. Res.,* **113,** D00A18, doi:10.1029/2008JD009982.

Sundaram, S., and L. Collins, 1997: Collision statistics in an isotropic particle-laden turbulent suspension. Part 1. Direct numerical simulations. *J. Fluid Mech.,* **335,** 75–109, doi:10.1017/S0022112096004454.

Vivekanandan, J., B. Martner, M. Politoich, and G. Zhang, 1999: Retrieval of atmospheric liquid and ice characteristics using dual-wavelength radar observations. *IEEE Trans. Geosci. Remote Sens.,* **37,** 2325–2334, doi:10.1109/36.789629.

Wang, L., and M. Maxey, 1993: Settling velocity and concentration distribution of heavy particles in homogeneous isotropic turbulence. *J. Fluid Mech.,* **256,** 27–68, doi:10.1017/S0022112093002708.

——, B. Rosa, H. Gao, G. He, and G. Jin, 2009: Turbulent collision of inertial particles: Point-particle based, hybrid simulations and beyond. *Int. J. Multiphase Flow,* **35,** 854–867, doi:10.1016/j.ijmultiphaseflow.2009.02.012.

Wang, Z., G. Heymsfield, L. Li, and A. Heymsfield, 2005: Retrieving optically thick ice cloud microphysical properties by using airborne dual-wavelength radar measurements. *J. Geophys. Res.,* **110,** D19201, doi:10.1029/2005JD005969.

Woittiez, E., H. Jonker, and L. Portela, 2009: On the combined effects of turbulence and gravity on droplet collisions in clouds: A numerical study. *J. Atmos. Sci.,* **66,** 1926–1943, doi:10.1175/2005JAS2669.1.

Yoshimoto, H., and S. Goto, 2007: Self-similar clustering of inertial particles in homogeneous turbulence. *J. Fluid Mech.,* **577,** 275–286, doi:10.1017/S0022112007004946.

Zaichik, L., and V. Alipchenkov, 2007: Refinement of the probability density function model for preferential concentration of aerosol particles in isotropic turbulence. *Phys. Fluids,* **19,** 113308, doi:10.1063/1.2813044.